A SECOND-ORDER NUMERICAL METHOD FOR LANDAU-LIFSHITZ-GILBERT EQUATION WITH LARGE DAMPING PARAMETERS

YONGYONG CAI, JINGRUN CHEN, CHENG WANG, AND CHANGJIAN XIE

ABSTRACT. A second order accurate numerical scheme is proposed and implemented for the Landau-Lifshitz-Gilbert equation, which models magnetization dynamics in ferromagnetic materials, with large damping parameters. The main advantages of this method are associated with the following features: (1) It only solves linear systems of equations with constant coefficients where fast solvers are available, so that the numerical efficiency has been greatly improved, in comparison with the existing Gauss-Seidel project method. (2) The second-order accuracy in time is achieved, and it is unconditionally stable for large damping parameters. Moreover, both the second-order accuracy and the great efficiency improvement will be verified by several numerical examples in the 1D and 3D simulations. In the presence of large damping parameters, it is observed that this method is unconditionally stable and finds physically reasonable structures while many existing methods have failed. For the domain wall dynamics, the linear dependence of wall velocity with respect to the damping parameter and the external magnetic field will be obtained through the reported simulations.

1. INTRODUCTION

Ferromagnetic materials are widely used for data storage due to the bi-stable states of the intrinsic magnetic order or magnetization. The dynamics of magnetization has been modeled by the Landau-Lifshitz-Gilbert (LLG) equation [9,13]. In particular, two terms are involved in the dynamics of the LLG equation: the gyromagnetic term, which is energetically conservative, and the damping term, which is energetically dissipative.

The damping term is important since it strongly affects the energy required and the speed at which a magnetic device operates. A recent experiment on a magnetic-semiconductor heterostructure [25] has indicated that the Gilbert damping constant can be adjusted. At the microscopic level, the electron scattering, the itinerant electron relaxation [11], and the phonon-magnon coupling [16,17] are responsible to the damping, which can be obtained from electronic structure calculations [19]. For the application purpose, tuning the damping parameter allows one to optimize the magneto-dynamic properties in the material, such as lowering the switching current and increasing the writing speed of magnetic memory devices [23].

While most experiments have been devoted to small damping parameters [4,14, 22], large damping effects are observed in [10,18]. The magnetization switching time

tends to be shorter in the presence of the large damping constant [18]. Extremely large damping parameters (~ 9) are presented in [10].

The LLG equation is a vectorial and nonlinear system with the fixed length of magnetization in a point-wise sense. Significant efforts have been devoted to design efficient and stable numerical methods for micromagnetics simulations; see [6,12] for reviews and references therein. Among the existing numerical works, semi-implicit schemes have been very popular since they avoid a complicated nonlinear solver while preserving the numerical stability; see [2,7,24], etc. In particular, the second-order accurate backward differentiation formula (BDF) scheme is constructed in [24], with a one-sided interpolation. In turn, a three-dimensional linear system needs to be solved at each time step, with non-constant coefficients. Moreover, a theoretical analysis of the second order convergence estimate has been established in [5] for such a BDF2 method. As another approach, a linearly implicit method in [2] introduces the tangent space to deal with the length constraint of magnetization, with the first-order temporal accuracy. As a further extension, high-order BDF schemes have been constructed and analyzed in a more recent work [1]. An unconditionally unique solvability of the semi-implicit schemes has been proved in [1,5], while the convergence analysis has required a condition that the temporal step-size is proportional to the spatial grid-size. However, an obvious disadvantage has been observed for these semi-implicit schemes: the vectorial structure of the LLG equation leads to a non-symmetric linear system at each time step, which cannot be implemented by an FFT-based fast solver. In fact, the GMRES is often used, while its efficiency depends heavily on the temporal step-size and the spatial grid-size, and extensive numerical experiments have indicated much more expensive computational costs than standard Poisson solvers [24].

The Gauss-Seidel projection method (GSPM) is another popular set of numerical algorithms since only linear systems with constant coefficients need to be solved at each time step [8,15,21]. This method is based on a combination of a Gauss-Seidel update of an implicit solver for the gyromagnetic term, the heat flow of the harmonic map, and a projection step to overcome the stiffness and the nonlinearity associated to the LLG equation. In this numerical approach, the implicit discretization is only applied to the scalar heat equation implicitly several times; therefore, the FFT-based fast solvers become available, due to the symmetric, positive definite (SPD) structures of the linear system. The original GSPM method [20] turns out to be unstable for small damping parameters, while this issue has been resolved in [8] with more updates of the stray field. Its numerical efficiency has been further improved by reducing the number of linear systems per time step [15]. One little deficiency of GSPM is its first-order accuracy in time.

Meanwhile, in spite of these improvements, the GSPM method is computationally more expensive than the standard Poisson solver, because of the Gauss-Seidel iteration involved in the algorithm. An additional deficiency of the GSPM is its first-order accuracy in time. Moreover, most of the above-mentioned methods have been mainly focused on small damping parameters with the only exception in a theoretical work [1]. In other words, there has been no numerical method designed specifically for real micromagnetics simulations with large damping parameters. In this paper, we propose a second-order accurate numerical method to solve the LLG equation with large damping parameters, whose complexity is also comparable to

solving the scalar heat equation. To achieve this goal, the LLG system is reformulated, in which the damping term is rewritten as a harmonic mapping flow. In turn, the constant-coefficient Laplacian part is treated by a standard BDF2 temporal discretization, and the associated dissipation will form the foundation of the numerical stability. Meanwhile, all the nonlinear parts, including both the gyromagnetic term and the remaining nonlinear expansions in the damping term, are computed by a fully explicit approximation, which is accomplished by a second order extrapolation formula. Because of this fully explicit treatment for the nonlinear parts, the resulting numerical scheme only requires a standard Poisson solver at each time step. This fact will greatly facilitate the computational efforts, since the FFT-based fast solver could be efficiently applied, due to the SPD structure of the linear system involved at each time step. In addition, the numerical stability has been demonstrated by extensive computational experiments, and these experiments has verified the idea that the dissipation property of the heat equation part would be able to ensure the numerical stability of the nonlinear parts, with large damping parameters.

The rest of this paper is organized as follows. In section 2, the micromagnetics model is reviewed, and the numerical method is proposed, as well as its comparison with the GSPM and the semi-implicit projection method (SIPM). Subsequently, the numerical results are presented in section 3, including the temporal and spatial accuracy check in both the 1D and 3D computations, the numerical efficiency investigation (in comparison with the GSPM and SIPM algorithms), the stability study with respect to the damping parameter, and the dependence of domain wall velocity on the damping parameter and the external magnetic field. Finally, some concluding remarks are made in section 4.

2. The physical model and the numerical method

2.1. **Landau-Lifshitz-Gilbert equation.** The LLG equation describes the dynamics of magnetization which consists of the gyromagnetic term and the damping term [3, 13]. In the nondimensionalized form, this equation reads as

$$(2.1) \qquad \boldsymbol{m}_t = -\boldsymbol{m} \times \boldsymbol{h}_{\text{eff}} - \alpha \boldsymbol{m} \times (\boldsymbol{m} \times \boldsymbol{h}_{\text{eff}})$$

with the homogeneous Neumann boundary condition

$$(2.2) \qquad \frac{\partial \boldsymbol{m}}{\partial \boldsymbol{\nu}}\bigg|_{\partial \Omega} = 0,$$

where Ω is a bounded domain occupied by the ferromagnetic material and $\boldsymbol{\nu}$ is unit outward normal vector along $\partial \Omega$.

In more details, the magnetization $\boldsymbol{m} : \Omega \subset \mathbb{R}^d \to \mathbb{R}^3, d = 1, 2, 3$ is a three-dimensional vector field with a pointwise constraint $|\boldsymbol{m}| = 1$. The first term on the right-hand side in (2.1) is the gyromagnetic term and the second term stands for the damping term, with $\alpha > 0$ being the dimensionless damping coefficient.

The effective field $\boldsymbol{h}_{\text{eff}}$ is obtained by taking the variation of the Gibbs free energy of the magnetic body with respect to $\boldsymbol{m}$. The free energy includes the exchange energy, the anisotropy energy, the magnetostatic energy, and the Zeeman energy:

$$(2.3) \qquad F[\boldsymbol{m}] = \frac{\mu_0 M_s^2}{2} \left\{ \int_\Omega \left(\epsilon |\nabla \boldsymbol{m}|^2 + q \left(m_2^2 + m_3^2 \right) - 2 \boldsymbol{h}_e \cdot \boldsymbol{m} - \boldsymbol{h}_s \cdot \boldsymbol{m} \right) \mathrm{d}\boldsymbol{x} \right\}.$$

Therefore, the effective field includes the exchange field, the anisotropy field, the stray field $\boldsymbol{h}_s$, and the external field $\boldsymbol{h}_e$. For a uniaxial material, it is clear that

$$(2.4) \qquad \boldsymbol{h}_{\text{eff}} = \epsilon\Delta\boldsymbol{m} - q(m_2\boldsymbol{e}_2 + m_3\boldsymbol{e}_3) + \boldsymbol{h}_s + \boldsymbol{h}_e,$$

where the dimensionless parameters become $\epsilon = C_{ex}/(\mu_0 M_s^2 L^2)$ and $q = K_u/(\mu_0 M_s^2)$ with L the diameter of the ferromagnetic body and μ_0 the permeability of vacuum. The unit vectors are given by $\boldsymbol{e}_2 = (0,1,0)$, $\boldsymbol{e}_3 = (0,0,1)$, and Δ denotes the standard Laplacian operator. For the Permalloy, an alloy of Nickel (80%) and Iron (20%), typical values of the physical parameters are given by: the exchange constant $C_{ex} = 1.3 \times 10^{-11}$ J/m, the anisotropy constant $K_u = 100$ J/m^3, the saturation magnetization constant $M_s = 8.0 \times 10^5$ A/m. The stray field takes the form

$$(2.5) \qquad \boldsymbol{h}_{\text{s}} = \frac{1}{4\pi}\nabla\int_\Omega \nabla\left(\frac{1}{|\boldsymbol{x}-\boldsymbol{y}|}\right)\cdot\boldsymbol{m}(\boldsymbol{y})\,d\boldsymbol{y}.$$

If Ω is a rectangular domain, the evaluation of (2.5) can be efficiently done by the Fast Fourier Transform (FFT) [20].

For brevity, the following source term is defined

$$(2.6) \qquad \boldsymbol{f} = -Q(m_2\boldsymbol{e}_2 + m_3\boldsymbol{e}_3) + \boldsymbol{h}_s + \boldsymbol{h}_e.$$

and the original PDE system (2.1) could be rewritten as

$$(2.7) \qquad \boldsymbol{m}_t = -\boldsymbol{m}\times(\epsilon\Delta\boldsymbol{m}+\boldsymbol{f}) - \alpha\boldsymbol{m}\times\boldsymbol{m}\times(\epsilon\Delta\boldsymbol{m}+\boldsymbol{f}).$$

Thanks to point-wise identity $|\boldsymbol{m}| = 1$, we obtain an equivalent form:

$$(2.8) \qquad \boldsymbol{m}_t = \alpha(\epsilon\Delta\boldsymbol{m}+\boldsymbol{f}) + \alpha\left(\epsilon|\nabla\boldsymbol{m}|^2 - \boldsymbol{m}\cdot\boldsymbol{f}\right)\boldsymbol{m} - \boldsymbol{m}\times(\epsilon\Delta\boldsymbol{m}+\boldsymbol{f}).$$

In particular, it is noticed that the damping term is rewritten as a harmonic mapping flow, which contains a constant-coefficient Laplacian diffusion term. This fact will greatly improve the numerical stability of the proposed scheme.

For the numerical description, we first introduce some notations for discretization and numerical approximation. Denote the temporal step-size by k, and $t^n = nk$, $n \leq \lfloor\frac{T}{k}\rfloor$ with T the final time. The spatial mesh-size is given by $h_x = h_y = h_z = h = 1/N$, and $\boldsymbol{m}_{i,j,\ell}^n$ stands for the magnetization at time step t^n, evaluated at the spatial location $(x_{i-\frac{1}{2}}, y_{j-\frac{1}{2}}, z_{\ell-\frac{1}{2}})$ with $x_{i-\frac{1}{2}} = \left(i-\frac{1}{2}\right)h_x$, $y_{j-\frac{1}{2}} = \left(j-\frac{1}{2}\right)h_y$ and $z_{\ell-\frac{1}{2}} = \left(\ell-\frac{1}{2}\right)h_z$ $(0 \leq i,j,\ell \leq N+1)$. In addition, a third order extrapolation formula is used to approximate the homogeneous Neumann boundary condition. For example, such a formula near the boundary along the z direction is given by

$$\boldsymbol{m}_{i,j,1} = \boldsymbol{m}_{i,j,0}, \quad \boldsymbol{m}_{i,j,N+1} = \boldsymbol{m}_{i,j,N}.$$

The boundary extrapolation along other boundary sections can be similarly made.

The standard second-order centered difference applied to $\Delta\boldsymbol{m}$ results in

$$\Delta_h\boldsymbol{m}_{i,j,k} = \frac{\boldsymbol{m}_{i+1,j,k} - 2\boldsymbol{m}_{i,j,k} + \boldsymbol{m}_{i-1,j,k}}{h_x^2}$$
$$+ \frac{\boldsymbol{m}_{i,j+1,k} - 2\boldsymbol{m}_{i,j,k} + \boldsymbol{m}_{i,j-1,k}}{h_y^2}$$
$$+ \frac{\boldsymbol{m}_{i,j,k+1} - 2\boldsymbol{m}_{i,j,k} + \boldsymbol{m}_{i,j,k-1}}{h_z^2},$$

and the discrete gradient operator $\nabla_h \boldsymbol{m}$ with $\boldsymbol{m} = (u, v, w)^T$ reads as

$$\nabla_h \boldsymbol{m}_{i,j,k} = \begin{bmatrix} \frac{u_{i+1,j,k} - u_{i-1,j,k}}{h_x} & \frac{v_{i+1,j,k} - v_{i-1,j,k}}{h_x} & \frac{w_{i+1,j,k} - w_{i-1,j,k}}{h_x} \\ \frac{u_{i,j+1,k} - u_{i,j-1,k}}{h_y} & \frac{v_{i,j+1,k} - v_{i,j-1,k}}{h_y} & \frac{w_{i,j+1,k} - w_{i,j-1,k}}{h_y} \\ \frac{u_{i,j,k+1} - u_{i,j,k-1}}{h_z} & \frac{v_{i,j,k+1} - v_{i,j,k-1}}{h_z} & \frac{w_{i,j,k+1} - w_{i,j,k-1}}{h_z} \end{bmatrix}.$$

Subsequently, the GSPM and the SIPM numerical methods need to be reviewed, which could be used for the later comparison.

2.2. The Gauss-Seidel projection method.

The GSPM is based on a combination of a Gauss-Seidel update of an implicit solver for the gyromagnetic term, the heat flow of the harmonic map, and a projection step. It only requires a series of heat equation solvers with constant coefficients; as a result, the FFT-based fast solvers could be easily applied. This method is first-order in time and second-order in space. Below is the detailed outline of the GSPM method in [8].

Step 1.   Implicit Gauss-Seidel:

$$g_i^n = (I - \epsilon \Delta t \Delta_h)^{-1} (m_i^n + \Delta t f_i^n), \quad i = 2, 3,$$
(2.9)
$$g_i^* = (I - \epsilon \Delta t \Delta_h)^{-1} (m_i^* + \Delta t f_i^*), \quad i = 1, 2,$$

(2.10)
$$\begin{pmatrix} m_1^* \\ m_2^* \\ m_3^* \end{pmatrix} = \begin{pmatrix} m_1^n + (g_2^n m_3^n - g_3^n m_2^n) \\ m_2^n + (g_3^n m_1^* - g_1^n m_3^n) \\ m_3^n + (g_1^* m_2^* - g_2^* m_1^*) \end{pmatrix}.$$

Step 2.   Heat flow without constraints:

(2.11)
$$\boldsymbol{f}^* = -Q(m_2^* \boldsymbol{e}_2 + m_3^* \boldsymbol{e}_3) + \boldsymbol{h}_s^* + \boldsymbol{h}_e,$$

(2.12)
$$\begin{pmatrix} m_1^{**} \\ m_2^{**} \\ m_3^{**} \end{pmatrix} = \begin{pmatrix} m_1^* + \alpha \Delta t (\epsilon \Delta_h m_1^{**} + f_1^*) \\ m_2^* + \alpha \Delta t (\epsilon \Delta_h m_2^{**} + f_2^*) \\ m_3^* + \alpha \Delta t (\epsilon \Delta_h m_3^{**} + f_3^*) \end{pmatrix}.$$

Step 3.   Projection onto S^2:

(2.13)
$$\begin{pmatrix} m_1^{n+1} \\ m_2^{n+1} \\ m_3^{n+1} \end{pmatrix} = \frac{1}{|m^{**}|} \begin{pmatrix} m_1^{**} \\ m_2^{**} \\ m_3^{**} \end{pmatrix}.$$

Here $\boldsymbol{m}^*$ denotes the intermediate values of $\boldsymbol{m}$, and stray fields $\boldsymbol{h}_s^n$ and $\boldsymbol{h}_s^*$ are evaluated at $\boldsymbol{m}^n$ and $\boldsymbol{m}^*$, respectively.

Remark 2.1. *Two improved versions of the GSPM have been studied in* [15], *which turn out to be more efficient than the original GSPM. Meanwhile, it is found that both improved versions become unstable when $\alpha > 1$, while the original GSPM (outlined above) is stable even when $\alpha \leq 10$. Therefore, we shall use the original GSPM in* [8] *for the numerical comparison in this work.*

2.3. **Semi-implicit projection method.** The SIPM has been outlined in [5, 24]. This method is based on the second-order BDF temporal discretization, combined with an explicit extrapolation. It is found that SIPM is unconditionally stable and is second-order accurate in both space and time. The algorithmic details are given as follows.

(2.14)
$$
\begin{cases}
\dfrac{\frac{3}{2}\tilde{\boldsymbol{m}}_h^{n+2} - 2\boldsymbol{m}_h^{n+1} + \frac{1}{2}\boldsymbol{m}_h^n}{k} = -\hat{\boldsymbol{m}}_h^{n+2} \times \left(\epsilon\Delta_h\tilde{\boldsymbol{m}}_h^{n+2} + \hat{\boldsymbol{f}}_h^{n+2}\right) \\
\quad - \alpha\hat{\boldsymbol{m}}_h^{n+2} \times \left(\hat{\boldsymbol{m}}_h^{n+2} \times (\epsilon\Delta_h\tilde{\boldsymbol{m}}_h^{n+2} + \hat{\boldsymbol{f}}_h^{n+2})\right), \\
\qquad\qquad \boldsymbol{m}_h^{n+2} = \dfrac{\tilde{\boldsymbol{m}}_h^{n+2}}{|\tilde{\boldsymbol{m}}_h^{n+2}|},
\end{cases}
$$

where $\tilde{\boldsymbol{m}}_h^{n+2}$ is an intermediate magnetization, and $\hat{\boldsymbol{m}}_h^{n+2}$, $\hat{\boldsymbol{f}}_h^{n+2}$ are given by the following extrapolation formula:

$$
\hat{\boldsymbol{m}}_h^{n+2} = 2\boldsymbol{m}_h^{n+1} - \boldsymbol{m}_h^n,
$$
$$
\hat{\boldsymbol{f}}_h^{n+2} = 2\boldsymbol{f}_h^{n+1} - \boldsymbol{f}_h^n,
$$

with $\boldsymbol{f}_h^n = -Q(m_2^n\boldsymbol{e}_2 + m_3^n\boldsymbol{e}_3) + \boldsymbol{h}_s^n + \boldsymbol{h}_e^n$. The presence of cross product in the SIPM yields a linear system of equations with non-symmetric structure and variable coefficients. In turn, the GMRES solver has to be applied to implement this numerical system. The numerical evidence has revealed that, the convergence of GMRES solver becomes slower for larger temporal step-size k or smaller spatial grid-size h, which makes the computation more challenging.

2.4. **The proposed numerical method.** The SIPM in (2.14) treats both the gyromagentic and the damping terms in a semi-implicit way, i.e., $\Delta\boldsymbol{m}$ is computed implicitly, while the coefficient functions are updated by a second order accurate, explicit extrapolation formula. The strength of the gyromagnetic term is controlled by $\Delta\boldsymbol{m} + \boldsymbol{f}$ since the length of $\boldsymbol{m}$ is always 1. Meanwhile, the strength of the damping term is controlled by the product of $\Delta\boldsymbol{m} + \boldsymbol{f}$ and the damping parameter α. For small α, say $\alpha \leq 1$, it is reasonable to treat both the gyromagentic and the damping terms semi-implicitly. However, for large α, an alternate approach would be more reasonable, in which the whole gyromagentic term is computed by an explicit extrapolation, while the nonlinear parts in the damping term is also updated by an explicit formula, and only the constant-coefficient $\Delta\boldsymbol{m}$ part in the damping term is implicitly updated. This idea leads to the proposed numerical method. To further simplify the presentation, we start with (2.8), and the numerical algorithm is proposed as follows.

(2.15)
$$
\begin{cases}
\dfrac{\frac{3}{2}\tilde{\boldsymbol{m}}_h^{n+2} - 2\boldsymbol{m}_h^{n+1} + \frac{1}{2}\boldsymbol{m}_h^n}{k} = -\hat{\boldsymbol{m}}_h^{n+2} \times \left(\epsilon\Delta_h\hat{\boldsymbol{m}}_h^{n+2} + \hat{\boldsymbol{f}}_h^{n+2}\right) \\
\quad + \alpha\left(\epsilon\Delta_h\tilde{\boldsymbol{m}}_h^{n+2} + \hat{\boldsymbol{f}}_h^{n+2}\right) \\
\quad + \alpha\left(\epsilon|\nabla_h\hat{\boldsymbol{m}}_h^{n+2}|^2 - \hat{\boldsymbol{m}}_h^{n+2} \cdot \hat{\boldsymbol{f}}_h^{n+2}\right)\hat{\boldsymbol{m}}_h^{n+2}, \\
\boldsymbol{m}_h^{n+2} = \dfrac{\tilde{\boldsymbol{m}}_h^{n+2}}{|\tilde{\boldsymbol{m}}_h^{n+2}|},
\end{cases}
$$

where

$$\hat{\boldsymbol{m}}_h^{n+2} = 2\boldsymbol{m}_h^{n+1} - \boldsymbol{m}_h^n,$$

$$\hat{\boldsymbol{f}}_h^{n+2} = 2\boldsymbol{f}_h^{n+1} - \boldsymbol{f}_h^n.$$

Table 1 compares the proposed method, the GSPM and the SIPM in terms of number of unknowns, dimensional size, symmetry pattern, and availability of FFT-based fast solver of linear systems of equations, and the number of stray field updates. At the formal level, the proposed method is clearly superior to both the GSPM and the SIPM algorithms. In more details, this scheme will greatly improve the computational efficiency, since only three Poisson solvers are needed at each time step. Moreover, this numerical method preserves a second-order accuracy in both space and time. The numerical results in section 3 will demonstrate that the proposed scheme provides a reliable and robust approach for micromagnetics simulations with high accuracy and efficiency in the regime of large damping parameters.

TABLE 1. Comparison of the proposed method, the Gauss-Seidel projection method, and the semi-implicit projection method.

Property or number	Proposed method	GSPM	SIPM
Linear systems	**3**	7	1
Size	$\boldsymbol{N^3}$	N^3	$3N^3$
Symmetry	**Yes**	Yes	No
Fast Solver	**Yes**	Yes	No
Accuracy	$\boldsymbol{\mathcal{O}(k^2 + h^2)}$	$\mathcal{O}(k + h^2)$	$\mathcal{O}(k^2 + h^2)$
Stray field updates	**1**	4	1

Remark 2.2. *To kick start the proposed method, one can apply a first-order algorithm, such as the first-order BDF method, in the first time step. An overall second-order accuracy is preserved in this approach.*

3. NUMERICAL EXPERIMENTS

In this section, we present a few numerical experiments with a sequence of damping parameters for the proposed method, the GSPM [8] and the SIPM [24], with the accuracy, efficiency, and stability examined in details. Domain wall dynamics is studied and its velocity is recorded in terms of the damping parameter and the external magnetic field.

3.1. **Accuracy and efficiency tests.** We set $\epsilon = 1$ and $\boldsymbol{f} = 0$ in (2.8) for convenience. The 1D exact solution is given by

$$\boldsymbol{m}_e = (\cos(X)\sin t, \sin(X)\sin t, \cos t)^T,$$

and the corresponding exact solution in 3D becomes

$$\boldsymbol{m}_e = (\cos(XYZ)\sin t, \sin(XYZ)\sin t, \cos t)^T,$$

where $X = x^2(1-x)^2$, $Y = y^2(1-y)^2$, $Z = z^2(1-z)^2$. In fact, the above exact solutions satisfy (2.8) with the forcing term $\boldsymbol{g} = \partial_t \boldsymbol{m}_e - \alpha\Delta\boldsymbol{m}_e - \alpha|\nabla\boldsymbol{m}_e|^2 + \boldsymbol{m}_e \times \Delta\boldsymbol{m}_e$, as well as the homogeneous Neumann boundary condition.

For the temporal accuracy test in the 1D case, we fix the spatial resolution as $h = 5D - 4$, so that the spatial approximation error becomes negligible. The damping parameter is taken as $\alpha = 10$, and the final time is set as $T = 1$. In the 3D test for the temporal accuracy, due to the limitation of spatial resolution, we take a sequence of spatial and temporal mesh sizes: $k = h_x^2 = h_y^2 = h_z^2 = h^2 = 1/N_0$ for the first-order method and $k = h_x = h_y = h_z = h = 1/N_0$ for the second-order method, with the variation of N_0 indicated below. Similarly, the damping parameter is given by $\alpha = 10$, while the final time T is indicated below. In turn, the numerical errors are recorded in term of the temporal step-size k in Table 2. It is clear that the temporal accuracy orders of the proposed numerical method, the GSPM, and the SIPM are given by 2, 1, and 2, respectively, in both the 1D and 3D computations.

The spatial accuracy order is tested by fixing $k = 1D - 5$, $\alpha = 10$, $T = 1$ in 1D and $k = 1D - 3$, $\alpha = 10$, $T = 1$ in 3D. The numerical error is recorded in term of the spatial grid-size h in Table 3. Similarly, the presented results have indicated the second order spatial accuracy of all the numerical algorithms, including the proposed method, the GSPM, and the SIPM, respectively, in both the 1D and 3D computations.

To make a comparison in terms of the numerical efficiency, we plot the CPU time (in seconds) vs. the error norm $\|\boldsymbol{m}_h - \boldsymbol{m}_e\|_\infty$. In details, the CPU time is recorded as a function of the approximation error in Figure 1a in 1D and in Figure 1b in 3D, with a variation of k and a fixed value of h. Similar plots are also displayed in Figure 1c in 1D and Figure 1d in 3D, with a variation of h and a fixed value of k. In the case of a fixed spatial resolution h, the proposed method is significantly more efficient than the GSPM and the SIPM in both the 1D and 3D computations. The SIPM is slightly more efficient than the GSPM, while such an advantage depends on the performance of GMRES, which may vary for different values of k and h. In the case of a fixed time step size k, the proposed method is slightly more efficient than the GSPM, in both the 1D and 3D computations, and the GSPM is more efficient than the SIPM.

3.2. **Stability test with large damping parameters.** To check the numerical stability of these three methods in the practical simulations of micromagnetics with large damping parameters, we consider a thin film of size $480 \times 480 \times 20\,\mathrm{nm}^3$ with grid points $100 \times 100 \times 4$. The temporal step-size is taken as $k = 1\,\mathrm{ps}$. A uniform state along the x direction is set to be the initial magnetization and the external magnetic field is set to be 0. Three different damping parameters, $\alpha = 0.01, 10, 40$, are tested with stable magnetization profiles shown in Figure 2. In particular, the following observations are made.

- The proposed method is the only one that is stable for very large damping parameters;
- All three methods are stable for moderately large α;
- The proposed method is the only one that is unstable for small α.

In fact, a preliminary theoretical analysis reveals that, an optimal rate convergence estimate of the proposed method could be theoretically justified for $\alpha > 3$. Meanwhile, extensive numerical experiments have implied that $\alpha > 1$ is sufficient to ensure the numerical stability in the practical computations.

Table 2. The numerical errors for the proposed method, the GSPM and the SIPM with $\alpha = 10$ and $T = 1$. Left: 1D with $h = 5D - 4$; Right: 3D with $k = h_x^2 = h_y^2 = h_z^2 = h^2 = 1/N_0$ for GSPM and $k = h_x = h_y = h_z = h = 1/N_0$ for the proposed method and SIPM, with N_0 specified in the table.

1D				3D			
k	$\lVert \cdot \rVert_\infty$	$\lVert \cdot \rVert_2$	$\lVert \cdot \rVert_{H^1}$	$k = h$	$\lVert \cdot \rVert_\infty$	$\lVert \cdot \rVert_2$	$\lVert \cdot \rVert_{H^1}$
4.0D-2	4.459D-4	5.226D-4	5.588D-4	1/20	6.171D-4	4.240D-4	4.246D-4
2.0D-2	1.147D-4	1.345D-4	1.436D-4	1/24	4.381D-4	3.010D-4	3.014D-4
1.0D-2	2.899D-5	3.402D-5	3.631D-5	1/28	3.268D-4	2.245D-4	2.248D-4
5.0D-3	7.192D-6	8.529D-6	9.119D-6	1/32	2.531D-4	1.739D-4	1.741D-4
2.5D-3	1.699D-6	2.321D-6	2.518D-6	1/36	2.017D-4	1.386D-4	1.387D-4
order	2.007	1.961	1.957	–	1.902	1.903	1.903

(A) Proposed method

1D				3D			
k	$\lVert \cdot \rVert_\infty$	$\lVert \cdot \rVert_2$	$\lVert \cdot \rVert_{H^1}$	$k = h^2$	$\lVert \cdot \rVert_\infty$	$\lVert \cdot \rVert_2$	$\lVert \cdot \rVert_{H^1}$
2.5D-3	2.796D-4	2.264D-4	1.445D-3	1/36	4.194D-4	2.683D-4	2.815D-4
1.25D-3	1.425D-4	1.174D-4	7.720D-4	1/64	2.388D-4	1.399D-4	1.500D-4
6.25D-4	7.170D-5	5.940D-5	4.026D-4	1/144	1.069D-4	6.106D-5	6.736D-5
3.125D-4	3.591D-5	2.971D-5	2.069D-4	1/256	6.021D-5	3.442D-5	3.860D-5
1.5625D-4	1.799D-5	1.488D-5	1.054D-4	1/400	3.855D-5	2.208D-5	2.501D-5
order	0.991	0.984	0.945	–	0.992	1.032	1.000

(B) GSPM

1D				3D			
k	$\lVert \cdot \rVert_\infty$	$\lVert \cdot \rVert_2$	$\lVert \cdot \rVert_{H^1}$	$k = h$	$\lVert \cdot \rVert_\infty$	$\lVert \cdot \rVert_2$	$\lVert \cdot \rVert_{H^1}$
4.0D-2	4.315D-4	5.111D-4	8.774D-4	1/20	6.170D-4	4.240D-4	4.249D-4
2.0D-2	1.128D-4	1.334D-4	2.255D-4	1/24	4.380D-4	3.010D-4	3.016D-4
1.0D-2	2.872D-5	3.399D-5	5.706D-5	1/28	3.268D-4	2.245D-4	2.251D-4
5.0D-3	7.174D-6	8.552D-6	1.433D-5	1/32	2.531D-4	1.739D-4	1.743D-4
2.5D-3	1.721D-6	2.333D-6	3.784D-6	1/36	2.017D-4	1.386D-4	1.389D-4
order	1.991	1.951	1.969	–	1.902	1.903	1.902

(C) SIPM

Under the same setup outlined above, we investigate the energy dissipation of the proposed method, the GSPM, and the SIPM. The stable state is attainable at $t = 2\,\text{ns}$, while the total energy is computed by (2.3). The energy evolution curves of different numerical methods with different damping parameters, $\alpha = 2, 5, 8, 10$, are displayed in Figure 3. One common feature is that the energy dissipation rate turns out to be faster for larger α, in all three schemes. Meanwhile, a theoretical derivation also reveals that the energy dissipation rate in the LLG equation (2.1) depends on α, and a larger α leads to a faster energy dissipation rate. Therefore, the numerical results generated by all these three numerical methods have made a nice agreement with the theoretical derivation.

TABLE 3. The numerical errors of the proposed method, the GSPM and the SIPM with $\alpha = 10$ and $T = 1$. Left: 1D with $k = 1D - 5$; Right: 3D with $k = 1D - 3$.

1D				3D			
h	$\|\cdot\|_\infty$	$\|\cdot\|_2$	$\|\cdot\|_{H^1}$	h	$\|\cdot\|_\infty$	$\|\cdot\|_2$	$\|\cdot\|_{H^1}$
4.0D-2	7.388D-3	7.392D-3	8.243D-3	1/2	4.261D-3	2.472D-3	2.472D-3
2.0D-2	1.848D-3	1.848D-3	2.061D-3	1/4	9.822D-4	5.595D-4	5.753D-4
1.0D-2	4.621D-4	4.621D-4	5.153D-4	1/8	2.453D-4	1.390D-4	1.424D-4
5.0D-3	1.155D-4	1.155D-4	1.288D-4	1/16	6.137D-5	3.471D-5	3.554D-5
order	2.000	2.000	2.000	–	2.035	2.047	2.037

(A) Proposed method

1D				3D			
h	$\|\cdot\|_\infty$	$\|\cdot\|_2$	$\|\cdot\|_{H^1}$	h	$\|\cdot\|_\infty$	$\|\cdot\|_2$	$\|\cdot\|_{H^1}$
4.0D-2	7.388D-3	7.392D-3	8.244D-3	1/2	4.256D-3	2.470D-3	2.470D-3
2.0D-2	1.848D-3	1.848D-3	2.061D-3	1/4	9.810D-4	5.589D-4	5.744D-4
1.0D-2	4.619D-4	4.622D-4	5.158D-4	1/8	2.447D-4	1.388D-4	1.423D-4
5.0D-3	1.153D-4	1.156D-4	1.302D-4	1/16	6.103D-5	3.468D-5	3.613D-5
order	2.000	2.000	1.995	–	2.037	2.047	2.030

(B) GSPM

1D				3D			
h	$\|\cdot\|_\infty$	$\|\cdot\|_2$	$\|\cdot\|_{H^1}$	h	$\|\cdot\|_\infty$	$\|\cdot\|_2$	$\|\cdot\|_{H^1}$
4.0D-2	7.388D-3	7.392D-3	8.243D-3	1/2	4.261D-3	2.472D-3	2.472D-3
2.0D-2	1.848D-3	1.848D-3	2.061D-3	1/4	9.822D-4	5.595D-4	5.753D-4
1.0D-2	4.621D-4	4.621D-4	5.153D-4	1/8	2.453D-4	1.390D-4	1.424D-4
5.0D-3	1.155D-4	1.155D-4	1.288D-4	1/16	6.137D-5	3.471D-5	3.554D-5
order	2.000	2.000	2.000	–	2.035	2.047	2.037

(C) SIPM

Meanwhile, we choose the same sequence of values for α, and display the energy evolution curves in terms of time up to $T = 2\,\text{ns}$ in Figure 4. It is found that the proposed method have almost the same energy dissipation pattern with the other two methods for moderately large damping parameters $\alpha = 2, 5, 8$. In the case of $\alpha = 10$, the SIPM has a slightly different energy dissipation pattern from the other two numerical methods.

3.3. **Domain wall motion.** A Neél wall is initialized in a nanostrip of size $800 \times 100 \times 4\,\text{nm}^3$ with grid points $128 \times 64 \times 4$. An external magnetic field of $\boldsymbol{h}_e = 5\,\text{mT}$ is then applied along the positive x direction and the domain wall dynamics is simulated up to $2\,\text{ns}$ with $\alpha = 2, 5, 8$. The corresponding magnetization profiles are visualized in Figure 5. Qualitatively, the domain wall moves faster as the value of α increases. Quantitatively, the corresponding dependence is found to be linear; see Figure 6. The slopes fitted by the least-squares method in terms of α and $\boldsymbol{h}_e$ are recorded in Table 4.

(A) Varying k in 1D up to $T = 1$

(B) Varying k in 3D up to $T = 0.1$

(C) Varying h in 1D up to $T = 1$
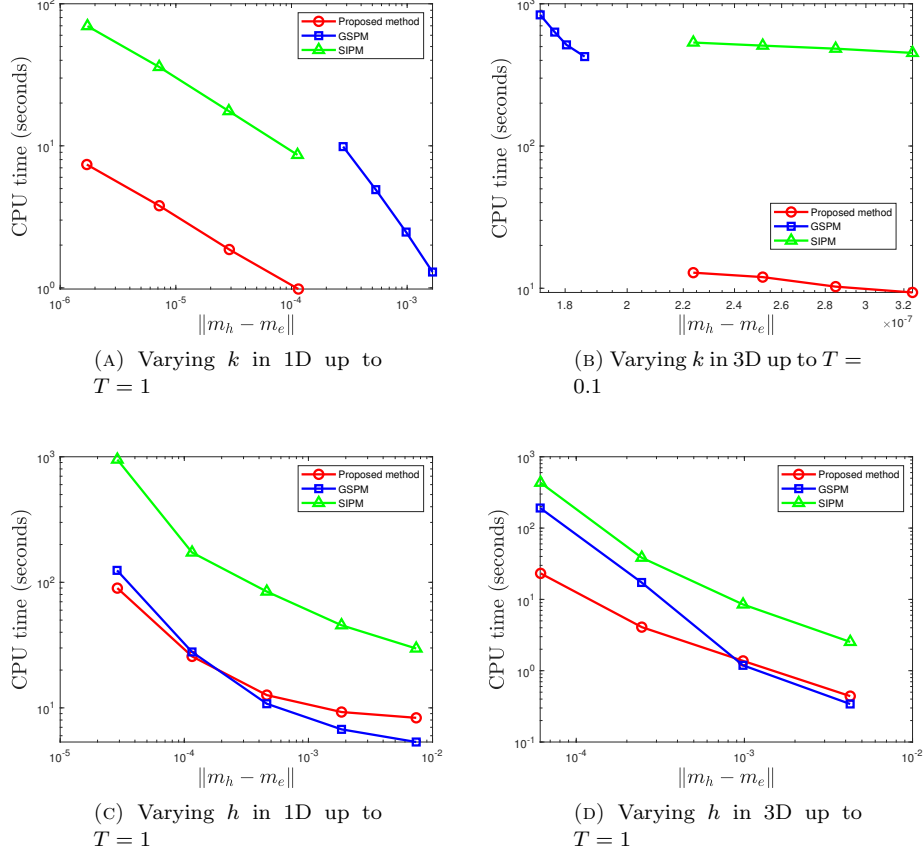
(D) Varying h in 3D up to $T = 1$

FIGURE 1. CPU time needed to achieve the desired numerical accuracy, for the proposed method, the GSPM and the SIPM, in both the 1D and 3D computations. The CPU time is recorded as a function of the approximation error by varying k or h independently. CPU time with varying k: proposed method < SIPM < GSPM; CPU time with varying h: proposed method $\lesssim\gtrsim$ GSPM < SIPM.

4. CONCLUSIONS

In this paper, we have proposed a second-order accurate numerical method to solve the Landau-Lifshitz-Gilbert equation with large damping parameters. For the numerical convenience, the LLG system is reformulated so that in which the damping term is rewritten as a harmonic mapping flow .This numerical scheme is based on the second-order backward-differentiation formula approximation for the temporal derivative, combined with an implicit treatment of the constant-coefficient diffusion term, and the fully explicit extrapolation approximation of the nonlinear terms, including the gyromagnetic term and the nonlinear part of the harmonic mapping flow. Thanks to the large damping parameter, the proposed method is verified
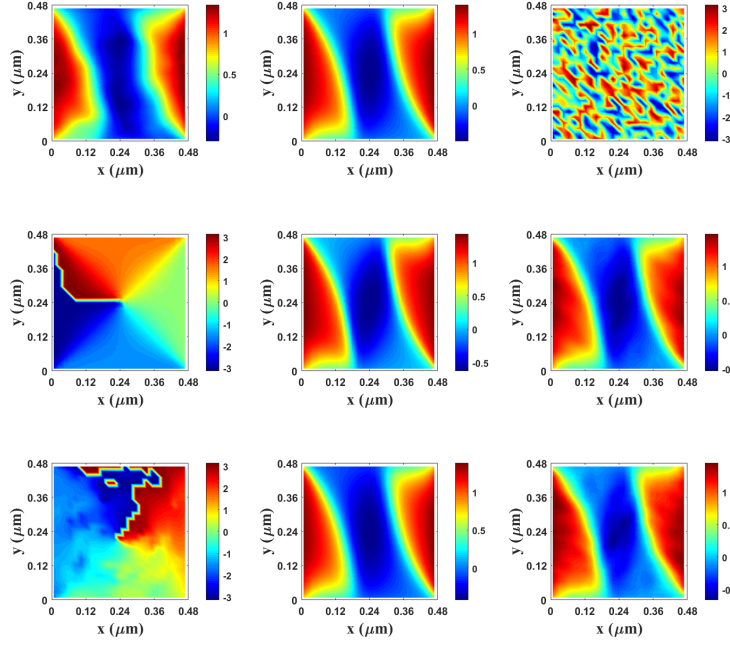
FIGURE 2. Stable structures in the absence of magnetic field at
2 ns when $\alpha = 0.01, 10, 40$. The color denotes the angle between the
first two components of the magnetization vector. Top: Proposed
method; Middle: GSPM; Bottom: SIPM. Left: $\alpha = 40$; Middle:
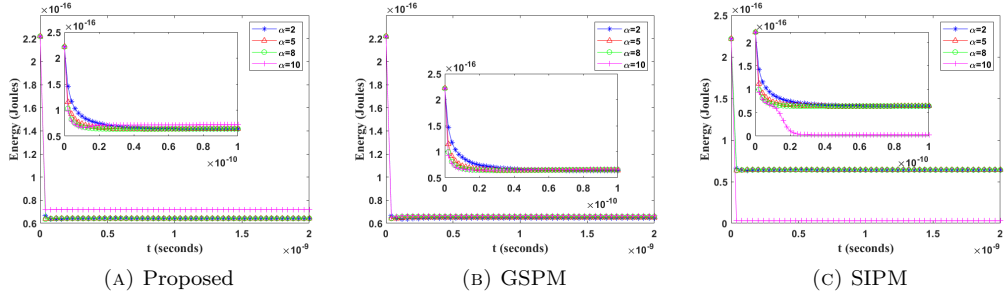$\alpha = 10$; Right: $\alpha = 0.01$.

(A) Proposed   (B) GSPM   (C) SIPM

FIGURE 3. Energy evolution curves of three numerical methods,
with different damping constants, $\alpha = 2, 5, 8, 10$, up to $t = 2$ ns in
the absence of external magnetic field. Left: Proposed numerical
method; Middle: GSPM; Right: SIPM. One common feature is
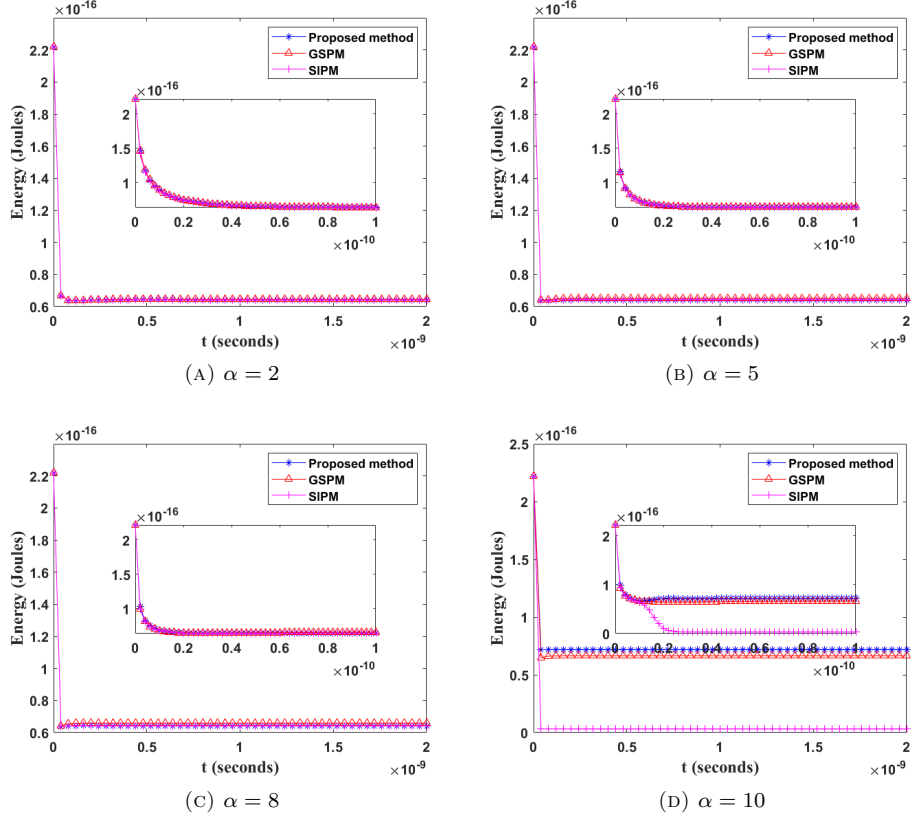that the energy dissipation rate is faster for larger α, which is
physically reasonable.

FIGURE 4. Energy evolution curves in terms of time, for the numerical results created by three numerical methods up to $t = 2\,\mathrm{ns}$ in the absence of external magnetic field for (a) $\alpha = 2$, (b) $\alpha = 5$, (c) $\alpha = 8$, and (d) $\alpha = 10$. The energy dissipation pattern of the proposed method is consistent with the other two methods for (a), (b), and (c), and the SIPM has a slightly different energy dissipation pattern from the other two methods for (d).

to be unconditionally stable. The proposed method is much more efficient than other semi-implicit schemes since only symmetric, positive definite linear systems of equations with constant coefficients need to be solved. Meanwhile, the proposed method is more accurate than the standard Gauss-Seidel projection method, due to its second-order accuracy in time. Numerical results in 1D and 3D are provided to demonstrate the accuracy and the efficiency of the proposed numerical method. In addition, micromagnetics simulations using the proposed method have provided physically reasonable structures and captured the linear dependence of the domain wall velocity with respect to the damping parameter. Therefore, the proposed method could be efficiently used for challenging practical simulations of micromagnetics with large damping parameters.
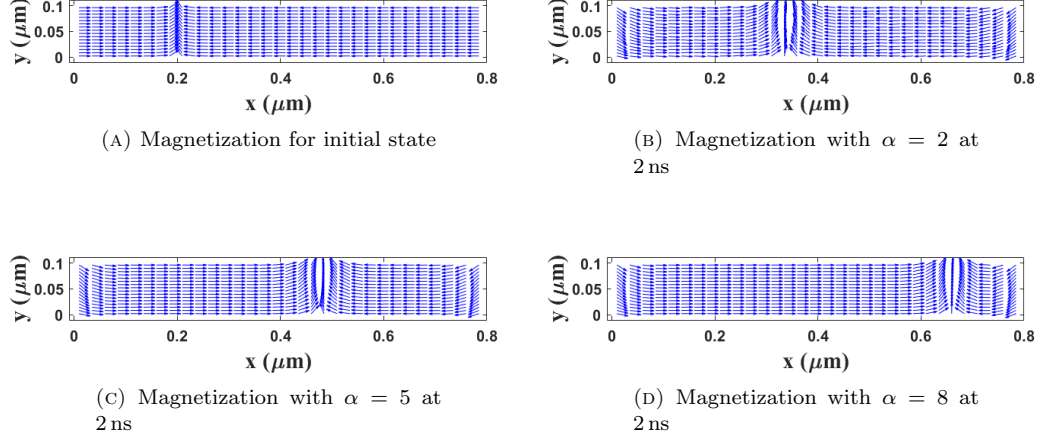
(A) Magnetization for initial state

(B) Magnetization with $\alpha = 2$ at 2 ns

(C) Magnetization with $\alpha = 5$ at 2 ns

(D) Magnetization with $\alpha = 8$ at 2 ns

FIGURE 5. Magnetization profiles of Neél wall motion in the presence of a magnetic field $\boldsymbol{h}_e = 5\,\mathrm{mT}$, with $\alpha = 2, 5, 8$ at 2 ns for the proposed numerical method. The in-plane arrow denotes the first two components of the magnetization vector. The wall moves faster for larger values of α and its velocity depends linearly on α.
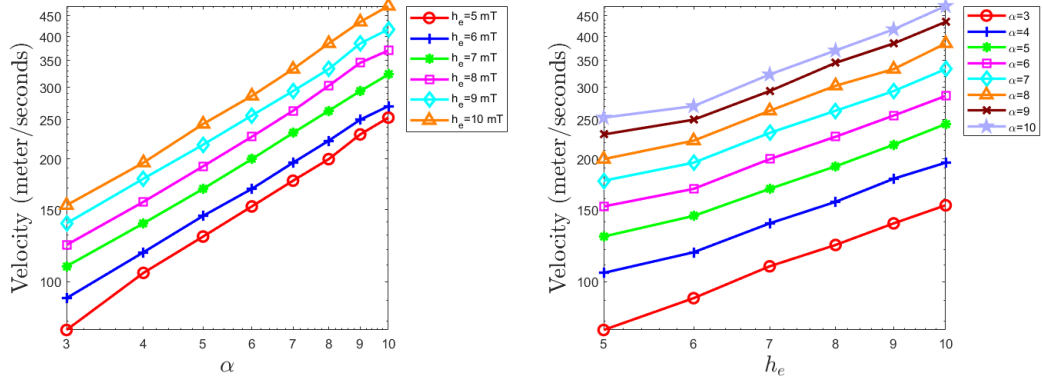

FIGURE 6. Linear dependence of the wall velocity with respect to the damping parameter α (left) and the external magnetic field $\boldsymbol{h}_e$ (right).

TABLE 4. Linear dependence of the domain wall velocity V in terms of the external magnetic field $\boldsymbol{h}_e$ and the damping parameter α.

V (m/s) $\quad \boldsymbol{h}_e$(mT) $\quad$ α	5	6	7	8	9	10	Slope
3	76	91	109	123	139	154	1.024
4	105	118	139	157	179	196	0.928
5	129	145	169	192	217	244	0.932
6	153	169	200	227	256	286	0.927
7	177	196	232	263	294	333	0.927
8	200	222	263	303	333	385	0.954
9	230	250	294	345	385	435	0.954
10	253	270	323	370	417	476	0.943
Slope	0.984	0.910	0.910	0.933	0.917	0.950	−

REFERENCES

[1] G. Akrivis, M. Feischl, B. Kovács, and C. Lubich, *Higher-order linearly implicit full discretization of the Landau-Lifshitz-Gilbert equation*, Math. Comp. **90** (2021), 995–1038.

[2] F. Alouges and P. Jaisson, *Convergence of a finite element discretization for the Landau-Lifshitz equations in micromagnetism*, Math. Models Methods Appl. Sci. **16** (2006), no. 02, 299–316.

[3] W.F. Brown, *Micromagnetics*, Interscience Tracts on Physics and Astronomy. Interscience Publishers (John Wiley and Sons), New York-London, 1963.

[4] S. Budhathoki, A. Sapkota, K.M. Law, B. Nepal, S. Ranjit, S. Kc, T. Mewes, and A. Hauser, *Low Gilbert damping and linewidth in magnetostrictive FeGa thin films*, J. Magn. Magn. Mater. **496** (2020), 165906.

[5] J. Chen, C. Wang, and C. Xie, *Convergence analysis of a second-order semi-implicit projection method for Landau-Lifshiz equation*, Appl. Numer. Math. (2021). Submitted and in review.

[6] I. Cimrák, *A survey on the numerics and computations for the Landau-Lifshitz equation of micromagnetism*, Arch. Comput. Methods Eng. **15** (2008), no. 3, 277–309.

[7] H. Gao, *Optimal error estimates of a linearized Backward Euler FEM for the Landau-Lifshitz equation*, SIAM J. Numer. Anal. **52** (2014), no. 5, 2574–2593.

[8] C.J. Garcıa-Cervera and W. E, *Improved Gauss-Seidel projection method for micromagnetics simulations*, J. Comput. Phys. **171** (2001), no. 1, 357–372.

[9] T.L. Gilbert, Phys. Rev. **100** (1955), 1243. [Abstract only; full report, Armor Research Foundation Project No. A059, Supplementary Report, May 1, 1956 (unpublished)].

[10] T.L. Gilbert and J.M. Kelly, *Anomalous rotational damping in ferromagnetic sheets*, Armour Research Foundation of Illinois Institute of Technology (1955). (unpublished).

[11] B. Heinrich, D. Fraítová, and V. Kamberský, *The influence of s-d exchange on relaxation of magnons in metals*, Phys. Stat. Solidi B-basic Solid Stat. Phys. **23** (1967), 501–507.

[12] M. Kruzík and A. Prohl, *Recent developments in the modeling, analysis, and numerics of ferromagnetism*, SIAM Rev. **48** (2006), no. 3, 439–483.

[13] L.D. Landau and E.M. Lifshits, *On the theory of the dispersion of magnetic permeability in ferromagnetic bodies*, Phys. Z. Sowjet. **63** (1935), no. 9, 153–169.

[14] D.M. Lattery, D. Zhang, J. Zhu, X. Hang, J. Wang, and X. Wang, *Low Gilbert damping constant in perpendicularly magnetized W/CoFeB/MgO films with high thermal stability*, Sci. Rep. **8** (2018), 13395.

[15] P. Li, C. Xie, R. Du, J. Chen, and X. Wang, *Two improved Gauss-Seidel projection methods for Landau-Lifshitz-Gilbert equation*, J. Comput. Phys. **401** (2020), 109046.

[16] T. Nan, Y. Lee, S. Zhuang, Z. Hu, J. Clarkson, X. Wang, C. Ko, H. Choe, Z. Chen, D. Budil, J. Wu, S. Salahuddin, J. Hu, R. Ramesh, and N. Sun, *Electric-field control of spin dynamics during magnetic phase transitions*, Sci. Adv. **6** (2020), no. 40, eabd2613.

[17] H. Suhl, *Theory of the magnetic damping constant*, IEEE Trans. Magn. **34** (1998), 1834–1838.

[18] T. Tanaka, S. Kashiwagi, Y. Otsuka, Y. Nozaki, Y. Hong, and K. Matsuyama, *Microwave-assisted magnetization reversal of exchange-coupled composite nanopillar with large Gilbert damping constant*, IEEE Tran. Magn. **50** (2014), 1–3.

[19] H. Tang and K. Xia, *Gilbert damping parameter in MgO-based magnetic tunnel junctions from first principles*, Phys. Rev. Applied **7** (2017), 034004.

[20] C. Wang and J.-G. Liu, *Convergence of gauge method for incompressible flow*, Math. Comp. **69** (2000), 1385–1407.

[21] X. Wang, C.J. García-Cervera, and W. E, *A Gauss-Seidel projection method for micromagnetics simulations*, J. Comput. Phys. **171** (2001), no. 1, 357–372.

[22] R. Weber, D. Han, I. Boventer, S. Jaiswal, R. Lebrun, G. Jakob, and M. Kläui, *Gilbert damping of CoFe-alloys*, J. Phys. D **52** (2019), 325001.

[23] D. Wei, *Micromagnetics and recording materials*, Springer Briefs in Apllied Sciences and Technology, Springer Berlin Heidelberg, 2012.

[24] C. Xie, C.J. García-Cervera, C. Wang, Z. Zhou, and J. Chen, *Second-order semi-implicit methods for micromagnetics simulations*, J. Comput. Phys. **404** (2020), 109104.

[25] D. Zhang, M. Li, L. Jin, C. Li, Y. Rao, X. Tang, and H. Zhang, *Extremely large magnetization and Gilbert damping modulation in NiFe/GeBi bilayers*, ACS Appl. Electron. Mater. **2** (2020), no. 1, 254–259.

School of Mathematical Sciences, Beijing Normal University, Beijing, China.
Email address: yongyong.cai@bnu.edu.cn

School of Mathematical Sciences, Soochow University, Suzhou, China.
Email address: jingrunchen@suda.edu.cn

Mathematics Department, University of Massachusetts, North Dartmouth, MA 02747, USA.
Email address: cwang1@umassd.edu

School of Mathematical Sciences, Soochow University, Suzhou, China.
Email address: 20184007005@stu.suda.edu.cn